Article - Control

TRANSACTIONS OF THE INSTITUTE OF MEASUREMENT & CONTROL

Transactions of the Institute of Measurement and Control
2023, Vol. 45(9) 1755–1768

DOI: 10.1177/01423312221140702
journals.sagepub.com/home/tim
SAGE

Application of bilateral sliding mode predictive compound control in photoelectric tracking system

Ren Yan[1,2] and Wang Yimin[3]

Abstract

This article focuses on the stable imaging problem of photoelectric imaging system that depends on the synchronous rotation of mirror and detector. When there is a relative movement between the mirror and the detector, it will cause image rotation, resulting in information loss and reduced tracking accuracy. It is difficult to achieve the high-precision synchronous movement between the mirror and the detector using the traditional unilateral control method. Different from the existing results of the traditional unilateral tracking method, this paper introduces the bilateral control structure in the field of robot teleoperation and proposes a novel compound control strategy based on the bilateral control structure. First, a robust disturbance observer is proposed to reduce the disturbance of the system, in which a new robust $H\infty$ mixed sensitivity control algorithm is designed to optimize the filter. Then, a novel generalized sliding mode predictive (NSMP) control strategy based on hybrid reaching law is proposed to eliminate the image rotation problem caused by time delay. Besides, a new power function is designed to replace the switching function in the reaching law to reduce chattering. Finally, the finite time theory and the Lyapunov theory are used to prove that the proposed control scheme can ensure that the system is stable and reach its steady state in a finite time. The simulation results show the effectiveness of the proposed control scheme.

Keywords

Stable imaging, bilateral control, sliding mode predictive control, robust $H\infty$ mixed sensitivity, finite time

Introduction

In recent years, high-coverage system and high-precision photoelectric imaging system are urgently required for target detection, target tracking, signal intelligence collection, land resource detection and many other fields (Ren et al., 2020; Wang et al., 2020). In the photoelectric imaging system, a 45° scan mirror is always set in front of the optical lens, which can effectively enhance the coverage. When the scanning mirror rotates the scanning image, if the motion is not synchronized with the imaging detector, image rotation problem will occur. The nonsynchronized rotation will cause the loss of image information and seriously affect the tracking accuracy of the target. There are two methods to solve the image rotation problem; the first method is digital image processing technology, which calculates the rotation angle between the rotated image and the original image and corrects it. However, due to the long processing time and large amount of calculation, it is not suitable for application in high dynamic photoelectric imaging systems (Giuffrida and Tsaftaris, 2020). Another method is a physical compensation method, which controls the scanning mirror motor and imaging detector to have their positions relatively static during the exposure time (Chang et al., 2019). As known, image rotation is caused by the movement asynchrony between the driving motors of the scanning mirror and the imaging detector; however, as reported, it is difficult to achieve high-precision synchronous movement between the two motors using the traditional unilateral control method.

In the field of robot teleoperation control, there is a kind of bilateral control (Chen et al., 2020). This method can control the two targets to maintain synchronous motion in the presence of communication delay, various non-linearities and uncertainty disturbance (Mobayen, 2018; Tajiri et al., 2018). The control system is divided into two parts: one is to estimate and compensate the disturbance; the other is to conduct a closed-loop controller for command tracking (Liu et al., 2020). In Tian et al. (2015), the bilateral control method based on position feedback and force feedback is applied to the photoelectric imaging system for the first time, and the image rotation is suppressed effectively. Therefore, the image

[1]School of Information Engineering, Inner Mongolia University of Science and Technology, China
[2]Key Laboratory of Airborne Optical Imaging and Measurement, Changchun Institute of Optics, Fine Mechanics and Physics, Chinese Academy of Sciences, China
[3]School of Marine Electrical Engineering, Dalian Maritime University, China

Corresponding author:
Wang Yimin, School of Marine Electrical Engineering, Dalian Maritime University, Dalian, China.
Email: 1780998621@qq.com

rotation can be effectively eliminated by applying the bilateral control method to the photoelectric imaging system. The design process of control system can be divided into two parts: the first part is the process of designing disturbance compensator for various disturbances; the second part is the process of designing closed-loop controller for target tracking. In this regard, this paper has carried out the following research.

To obtain better control performance, disturbance observer (DOB) is usually added to the control scheme to estimate the disturbance of the system. In this aspect, extended state observer (ESO) has been widely used in various fields because it has the advantages of simple structure and strong robustness (Fan et al., 2020). However, it is difficult to realize in practice. The sliding mode disturbance observer (SMDO) regards the non-linear disturbed as a kind of motion characteristic on the sliding mode and applies the difference between the output of the nominal model and the actual output as an equivalent disturbance to the nominal model (Yao et al., 2014), which enables a quick estimation and compensation, in turn, to the disturbance in the finite time. While the algorithm of sliding mode control is widely used in control systems because it is simple, it does not need to rely on the accurate system model and has the invariance to the parameter change and the external disturbance. However, sliding mode control has chattering problem, which seriously restricts its applicability and development (Ullah and Pei, 2020). Furthermore, the DOB can effectively estimate and compensate the system disturbance, but it is not practical in most cases to rely on the accurate mathematical model (Ding et al., 2020).

To solve the problems discussed above, robust disturbance observer (RDOB) is designed. This control method optimizes the filter in the DOB through robust $H\infty$ mixed sensitivity control (RHMS). It will show that the performance of the RDOB is less dependent on accurate mathematical model compared with traditional DOB, and calculation of the inverse of solution model is avoided. Therefore, it has better estimation performance and generality for interference.

As we all know, sliding mode variable structure control (SMC) is applied in many fields because of its good robustness and rapidity (Hu et al., 2020). It is an effective control method for uncertain system. However, chattering is an unavoidable problem in the design of sliding mode control. From the viewpoint of theoretical research, some interesting results of weakening chattering have been presented. Labbadi and Moussaoui (2021) designed fractional-order sliding mode control to reduce chattering. Huerta et al. (2021) developed high-order sliding mode control schemes to suppress chattering. Although the above two control methods can reduce chattering, the design process is complex and the implementation cost is too high in practical application. The authors in Cecilia et al. (2021) proposed the integral sliding mode control strategy to suppress chattering, but this control method also has a steady-state error. The authors in Chen et al. (2021) designed a Hybrid Reaching Law (HRL) algorithm, combining exponential reaching law and power reaching law, to alleviate the chattering problem in the Exponential Reaching Law. Wang et al. 2019(a) focused on a New Reaching Law (NRL). The NRL incorporates the power term and switching gain term of system state variables into the Conventional Exponential Reaching Law (CERL) and eventually suppresses the sliding mode chattering and increases the convergence rate of system state reaching the sliding mode surface. Zhang et al. 2019(a) developed a novel chatter-free reaching law, in which, as the switching gain was replaced by an adaptive function, chattering on the sliding surface tended to zero.

In addition, the imaging process of the photoelectric imaging system will have a time delay (TD) of about 20 ms. Although the common sliding mode control has good stability and fast convergence, it has some limitations on the applications to the photoelectric imaging system with TD. TD is always a hot and difficult problem in photoelectric imaging system. From the viewpoint of theoretical research, some interesting results of suppressing TD have been presented. At present, the common control methods to suppress TD can be roughly divided into two categories. One is based on Lyapunov stability theory to solve the controller. Han (2021) and Mobayen and Tchier (2017) proposed a linear matrix inequality (LMI)-based adaptive TD sliding mode control algorithm. The authors in Fang et al. (2021) developed an SMC law to force system trajectories onto the specified switching sliding surface in a finite time. Zhang et al. 2019(b) studied the sliding mode control scheme for a class of linear systems with uncertainty and time-varying delay. Xia and Jia (2003) designed a sliding surface function combined with artificial delay to enhance the dynamic performance of the power system. All of the above are based on Lyapunov–Krasovskii and Lyapunov–Razumikhin functions to derive the stability conditions and controllers for systems with TD. The other is predictive control, which can compensate the influence of TD by predicting the change of state variables in the range of TD. SMC has strong robustness because it is insensitive to system parameters and disturbances. This control method is very sensitive to the state change of the system, and its discontinuous switching control may affect the unmodeled characteristics of the system, thus damaging the system performance and causing instability. Therefore, it is not advisable to directly apply the sliding mode control method to the TD system. Prediction and delay compensation for linear systems are inherently more challenging, and while there are fewer results developed for such systems, there has been recent progress. Ovaska and Vainio (1997) proposed a nearly all-pass narrow-band predictor to be used as a predictive compensator of the computing delay. Gao et al. (2020) proposed a new direct compensation method (DCO) by predicting the current variation within the delay time. The authors in Truong et al. (2013) proposed a novel TD prediction method to forecast the system delay in the next working step for adjusting the sampling period to eliminate the bad effects of TD on the control performance. Yao et al. (2022) proposed a new weight-average-prediction (WAP) controller to compensate the delayed system states. The TD differential term is added to the control law, which transforms the traditional TD small signal model into a neutral TD mathematical model. Therefore, the predictive control scheme can effectively compensate the delay by predicting the state of the system information in the process of delay. However, to make the system have better robustness, it is very necessary to carry out further anti-interference control for the system. Therefore, some researchers have proposed a sliding mode predictive control scheme. Zhang et al. 2021(a) proposed a distributed model-free sliding mode predictive control strategy based on TD compensation technology to eliminate the influence of TD on the multi-agent systems (MASs), which can actively compensate for TD while ensuring system stability and consensus tracking performance requirements. Yang et al. (2020) designed a novel sliding mode prediction fault-tolerant control algorithm for multi-delay discrete uncertain systems with sensor fault. Zhang et al. 2021(b) designed a novel sliding mode prediction fault-tolerant control method to reduce the impact of TD on a class of discrete uncertain quad-rotor systems with multi-delays and actuator faults. The above sliding mode predictive control algorithms can reduce the impact of TD on the system, but the process of calculating the minimum cost function is cumbersome and has limitations. Compared with the above methods, we propose novel generalized sliding mode predictive (NSMP) does not need minimization cost function and accurate mathematical model, and has a wider application. In short, the above work shows that the sliding mode predictive control can effectively solve the problem of TD (Teng et al., 2019; Wang et al., 2019(a)).

The objective of this paper is to provide the theoretical analysis on image rotation compensation with bilateral control structure. The main contributions of this paper are fourfold.

1. The reason of image rotation and the structure of photoelectric imaging system are analysed. The bilateral control structure in the field of robot teleoperation is applied to the photoelectric imaging system. Therefore, a dual-channel bidirectional control structure based on the photoelectric imaging system is designed. This structure can make the two systems move synchronously so as to weaken the image rotation problem.
2. A novel RDOB based on RHMS is proposed. S/KS S: Sensitivity function, K: controller, KS: controller multiplied by sensitivity function hybrid method is used to optimize the DOB filter. The advantages are as follows. First, the design process is simplified. Second, solving the inverse problem of the model is avoided, and the application value and the estimation accuracy of interference are improved. According to the author's research, this hybrid method is used to design the DOB filter for the first time.
3. An NSMP based on mixed reaching law scheme is proposed. First, the New Mixed Reaching Law (NMRL) is proposed. The NMRL is composed of exponential approach rate and double power approach rate to ensure the global fast convergence of the system. Moreover, Generalized Predictive Control (GPC) is introduced into the sliding mode control in a novel form to constitute a sliding mode controller with predictive function. This controller combines the advantages of sliding mode control and GPC, and makes up for the limitations of sliding mode control in systems with TD. It can effectively reduce the impact of TD and improve the tracking speed of the system. Besides, a novel power function is used to replace the switching function in the NMRL to weaken the system chatter and enhance the tracking accuracy of the system. To the best knowledge of the authors, this is the first time to combine in such a novel way the generalized control and sliding mode control. The control strategy does not need accurate mathematical model and calculation of minimum cost function, which reduces the computational complexity and improves the universality of application.
4. Under the condition of discrete linear time-invariant system, the stability and finite time convergence of the system are proved under the control method proposed in this paper. And the upper bound of convergence time is proved. Finally, the error is quantified.

The rest of this paper is organized as follows. Section 'Bilateral control system' gives the overall control structure of the photoelectric imaging system and briefly describes the meaning of each component in the structure. Section 'System model' gives the system model. In section 'Design and analysis of disturbance', the robust DOB based on RHMS control will be designed. And the NSMP is proposed in section 'Design of sliding mode predictive controller'. Simulation experiment are carried out in section 'Experimental simulation and analysis'. Finally, section "Conclusion" will present conclusions.

Bilateral control system

The double-channel bilateral control structure of the photoelectric imaging system is shown in Figure 1. As shown in the figure, the bilateral control system is divided into two parts: the upper part represents, in block diagram form, the scanning agency and the lower part represents the compensation agency; they facilitate the control of rotation of the scan mirror and the imaging detector, respectively. Both the scanning agency and the compensation agency implement closed-loop control combined with DOBs, in which the closed-loop controllers adopt NSMP scheme to ensure the tracking performance of the system, while the observers are designed according to the criteria of the RDOB to eliminate noises such as model errors, external disturbances and carrier oscillations. The reference trajectory softens the system so that the system can smoothly reach the given value.

In Figure 1, yr_s denotes the reference input of the scan mirror system, uf_S denotes the closed-loop controller output of the scan mirror system, u_S denotes the control input of scan mirror system and d_S denotes the equivalent disturbance of the scan mirror system, including wind resistance moment, mass imbalance moment and so on. y_s denotes the measurement output of the scan mirror system, $\hat{d}_S$ denotes the disturbance estimate of the scan mirror system, yr_I denotes the reference input of the imaging detector system, uf_I denotes the closed-loop controller output of the imaging detector system, u_I denotes the control input of the imaging detector system and d_I denotes the equivalent disturbance of the imaging detector system, including wind resistance moment, mass imbalance moment and so on. $\hat{d}_I$ denotes the disturbance estimate of the imaging detector system, and y_I denotes the measurement output of the imaging detector system.

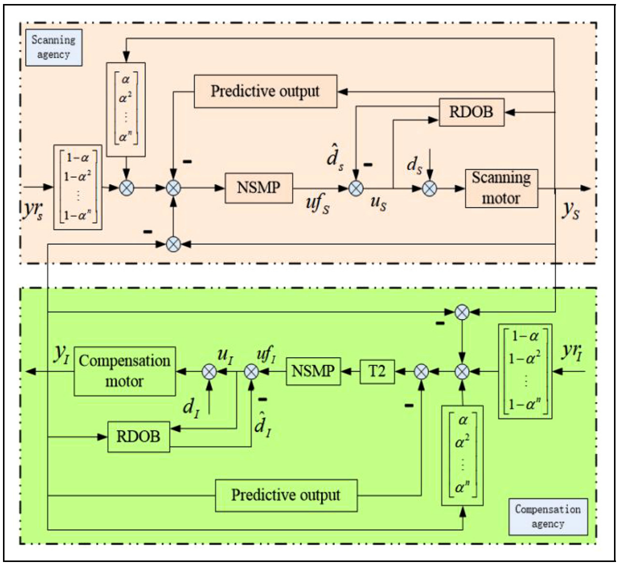

Figure 1. Double-channel bilateral control structure.

During the operation of the system, there is a TD from the detection of the target by the imaging detector to the reception of the deviation signal by the servo controller. It is the sum of a TD, accounting for photoelectric conversion delay, signal processing delay and communication transmission delay. To reduce the influence of the TD, the time required for miss distance is calculated by artificially delaying the feedback channel signal so that the input channel delay of miss distance can be equivalent to the control channel delay of imaging detector system, which is finally T2.

System model

The photoelectric imaging system is mainly composed of DC torque motor, encoder, pulse width modulation (PWM) power amplifier, position measuring device, platform frame and the optical system that is mounted on the frame. According to the motion characteristics, the motor models of the scanning mirror motor and the imaging detector motor can be simplified into the following form

$$J_s\ddot{\theta}_s = -B_s\dot{\theta}_s + u_s + \Delta_s(\theta, t) \tag{1}$$

$$J_I\ddot{\theta}_I = -B_I\dot{\theta}_I + u_I + \Delta_I(\theta, t) \tag{2}$$

where θ_s,$\dot{\theta}_s$ and $\ddot{\theta}_s$ are the angular position, angular speed and angular acceleration of the scan mirror system, respectively. J_s and B_s are the moment of inertia and the viscous damping coefficient of the scan mirror system, respectively. u_s is the control input of the scan mirror system, and $\Delta_s(\theta, t)$ is the unknown non-linear dynamic of the scan mirror system. θ_I,$\dot{\theta}_I$ and $\ddot{\theta}_I$ are the angular position, angular speed and angular acceleration of the imaging detector system, respectively. J_I and B_I are the moment of inertia and the viscous damping coefficient of the imaging detector system, respectively. u_I is the control input of the imaging detector system, and $\Delta_I(\theta, t)$ is the unknown non-linear dynamic of the imaging detector system.

The following content uses i instead of S and I for convenience. When subscript i is I, it indicates the variable of the imaging detector system. When subscript i is S, it indicates the variable of the scan mirror system. According to equations (1) and (2), the system transfer function can be described as

$$G_i(s) = \frac{Y_i(s)}{U_i(s)} = \frac{1}{J_i s^2 + B_i s} \tag{3}$$

The discrete model of the system is

$$G_i(z^{-1}) = \frac{y_i(k)}{u_i(k)} = \frac{z^{-1}(b_{i0} + b_{i1}z^{-1})}{a_{i0} + a_{i1}z^{-1} + a_{i2}z^{-2}} = z^{-1}\frac{B_i(z^{-1})}{A_i(z^{-1})} \tag{4}$$

where $A_i(z^{-1})$ and $B_i(z^{-1})$ are z^{-1} polynomials of order 2 and 1 of i system, respectively.$A_i(z^{-1}) = a_{i0} + a_{i1}z^{-1} + a_{i2}z^{-2}$ and $B_i(z^{-1}) = b_{i0} + b_{i1}z^{-1}$. a_{i0}, a_{i1}, a_{i2}, b_{i0}, b_{i1} are constants of i system.

Design and analysis of disturbance

In practice, uncertainty of the model and external disturbance are main factors influencing the stability of the line of sight (LoS) of the photoelectric imaging system. Disturbance compensation controller is developed to suppress external disturbance and uncertainties in this section.

DOB uses the inverse of the model and a low-pass filter to estimate the equivalent disturbance of the system. The low-pass filter reflects the system's ability to suppress the high-frequency noise. However, the process of designing a low-pass filter is tedious. In the design process, every time the low-pass filter is selected to test the robustness of the system.

To simplify the design process and optimize the low-pass filter, the RHMS function S/KS is used to the design the low-pass filter. The process is as follows.

RHMS control

The basic idea of robust control can be understood as to design the optimal controller by analysing the maximum bearing capacity of the system model with uncertainties. On the basis of this control, an optimization method called RHMS is further studied. The controller obtained by this method can simultaneously consider multiple design indexes, such as tracking accuracy, anti-interference performance and robust stability. Its basic structure is shown in Figure 2.

In Figure 2, w, e and y are reference signal, tracking error and measurement output respectively; u is the control input. W_s, W_R and W_T are weighted functions. $G(z^{-1})$ represents the controlled object. z_1, z_2 and z_3 are the performance signals of the system, and $P(z^{-1})$ is a generalized controlled object. $K(z^{-1})$ represents robust controller. z_1, z_2, and z_3 are system performance signals. The standard control forms are as follows

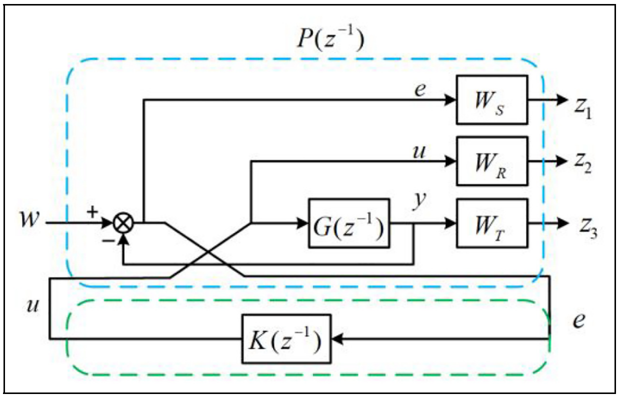

Figure 2. Mixed sensitivity control structure diagram.

$$\begin{bmatrix} z \\ e \end{bmatrix} = P(z^{-1}) \begin{bmatrix} w \\ u \end{bmatrix} = \begin{bmatrix} P_{11}(z^{-1}) & P_{12}(z^{-1}) \\ P_{21}(z^{-1}) & P_{22}(z^{-1}) \end{bmatrix} \begin{bmatrix} w \\ u \end{bmatrix} \tag{5}$$

where $z = [z_1\ z_2\ z_3]^T$, $P_{11} = [W_s\ -W_s G(z^{-1})]$, $P_{12} = [0\ \ W_R]$, $P_{21} = [0\ \ W_T G(z^{-1})]$ and $P_{22} = [1\ \ -G(z^{-1})]$.

The controller of RHMS is obtained by minimizing the infinite norm of $T_{zw\infty}$. It can be described as

$$\min_{K(z^{-1})} \|T_{zw}\|_\infty = \min_{K(z^{-1})} \left\| \begin{matrix} W_s(1 + G(z^{-1})K(z^{-1}))^{-1} \\ W_R K(z^{-1})(1 + G(z^{-1})K(z^{-1}))^{-1} \\ W_T G(z^{-1})K(z^{-1})(1 + G(z^{-1})K(z^{-1}))^{-1} \end{matrix} \right\|_\infty \tag{6}$$

There are usually the following definitions

$$S = \frac{1}{(1 + G(z^{-1})K(z^{-1}))} \tag{7}$$

$$T = G(z^{-1})K(z^{-1})/(1 + G(z^{-1})K(z^{-1})) \tag{8}$$

where S and T are the sensitivity function and complementary sensitivity function, respectively, which reflect the system's ability to suppress the low-frequency disturbance and the high-frequency disturbance respectively.

The weighting function is as follows

$$W_s = \frac{[(1 + \omega_0) - e^{-A\omega_0 T} z^{-1}]}{(M - Me^{-A\omega_0 T} \cdot z^{-1})} \tag{9}$$

$$W_R = const \tag{10}$$

$$W_T = \frac{\left(1 + \frac{\omega_0}{M} - A - e^{-A\omega_0 T} z^{-1}\right)}{(A - Ae^{-A\omega_0 T} z^{-1})} \tag{11}$$

where $A < 1$ denotes the maximum allowable steady-state error, ω_0 is the expected bandwidth, M is the peak value of sensitivity and T represents the sampling period. The smaller the A, the stronger the ability of the controller to suppress low-frequency disturbances.

Remark 1: W_s is the weighted function of the sensitivity function S, and the sensitivity function represents the transfer function from the disturbance input d to the measurement output y. It is also a transfer function from the reference signal w to the tracking error e. Because the external interference signal is usually of low frequency and the smaller the tracking error is expected, the better. Therefore, the low-frequency gain of S should be small, that is, the low-frequency gain of W_s should be large. Therefore, the smaller the A value, the stronger the ability of the controller to suppress low-frequency and high-frequency interference. W_T is the weighted function of the complementary sensitivity function T. T indicates the system's ability to suppress high-frequency noise. Generally, the smaller T, the better the suppression effect. In addition, due to the existence of identity relation $S + T = 1$, it is necessary to compromise in the design process.

RDOB design

To simplify the design process of DOB and improve the estimation accuracy of DOB to various disturbances, RHMS control is used to optimize the DOB filter. The designed filter is a low-pass filter, so the influence of high-frequency noise on the system can be ignored in the design process. So the robust H-infinity S/KS hybrid sensitivity method is used to optimize the filter. The equivalent deformation of the structure of DOB control based on RHMS is shown in Figure 3. Define the filter as

$$Q_i(z^{-1}) = \frac{L_i(z^{-1})}{1 + L_i(z^{-1})} = \frac{G_i(z^{-1})K_i(z^{-1})}{1 + G_i(z^{-1})K_i(z^{-1})} \tag{12}$$

where $Q_i(z^{-1})$ denotes the low-pass filter of i system, $K_i(z^{-1})$ is robust controller of i system and $L_i(z^{-1})$ is defined as the open-loop transfer function as follows

$$L_i(z^{-1}) = G_i(z^{-1})K_i(z^{-1}) \tag{13}$$

Then the sensitivity function is

$$S_i = \frac{1}{1 + L_i(z^{-1})} \tag{14}$$

$$S_i \cdot K_i(z^{-1}) = \frac{K_i(z^{-1})}{1 + L_i(z^{-1})} \tag{15}$$

According to the theory of RHMS, the sufficient conditions for the system to be stable are as follows

$$\left\| \begin{matrix} W_{is}S_i \\ W_{iR}K_i(z^{-1})S_i \end{matrix} \right\|_\infty < \gamma \tag{16}$$

where W_{is} and W_{iR} are the weight functions of S and KS, respectively. Equation (16) is the evaluation function for realizing the optimal disturbance suppression performance of DOB and ensuring the robustness of the system. Although it is difficult to determine whether γ is the minimum to the cases being dealt with, and the suboptimal γ works in practice regarding the infinite norm of the evaluation function.

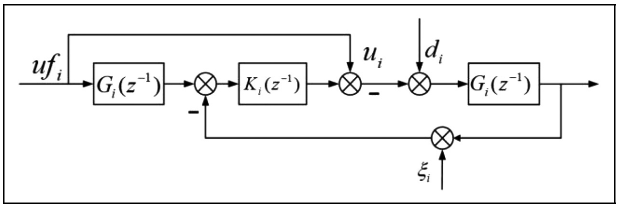

Figure 3. DOB control structure based on mixed sensitivity.

Design of sliding mode predictive controller

To deal with the problems of the image rotation caused by TD, an NSMP control is proposed, in which the system is enabled to predict its current output status within TD. This scheme can overcome the TD, so the image rotation can be eliminated.

The NSMP controller design consists of the following steps:

Step A: Setting up the corresponding Controlled Auto-Regressive Integral Moving Average (CARIMA) model.
Step B: Deriving the equation for the j-step ahead of output prediction on the basis of Diophantine equation.
Step C: Designing the predictive sliding surface and the sliding mode predictive controller on the basis of the first two steps.

CARIMA model

Start from the uses of the CARIMA model to predict the output value of the system in TD according to the historical data and control input (Bentsman and Ordys, 1999). Rewrite the system model (4) into CARIMA model form

$$A_i(z^{-1})y_i(k) = B_i(z^{-1})u_i(k-1) + C_i(z^{-1})\xi_i(k)/\Delta \tag{17}$$

where $C_i(z^{-1})$ is the n-order polynomial of z^{-1}, and $\Delta = 1 - z^{-1}$ is the backward difference operator. Let $\xi_i(k)$ be the white noise sequence with zero mean value. For simplicity, let $C_i(z^{-1}) = 1$.

J-step Prediction Output

According to the GPC theory, move on from Step A to predict the output ahead of j steps. Diophantine equation is as follows (Ogunye, 1999)

$$1 = E_i(z^{-1})A_i(z^{-1})\Delta + z^{-j}F_i(z^{-1}) \tag{18}$$

where $E_i(z^{-1}) = e_{i0} + e_{i1}z^{-1} + \cdots + e_{i\cdot j-1}z^{-j+1}$ and $F_i(z^{-1}) = f_{i0} + f_{i1}z^{-1} + \cdots + f_{i\cdot j-1}z^{-n}$. It can be seen that $E_i(z^{-1})$ and $F_i(z^{-1})$ are uniquely determined by the prediction steps j and $A_i(z^{-1})$.

Multiplying the two sides of equation (15) by $E_i(z^{-1})$, one has

$$\begin{aligned} E_i(z^{-1})A_i(z^{-1})\Delta y_i(k) = E_i(z^{-1})B_i(z^{-1})\Delta u_i(k-1) \\ + E_i(z^{-1})C_i(z^{-1})\xi_i(k) \end{aligned} \tag{19}$$

Define $G_{ij}(z^{-1})$ as

$$\begin{aligned} G_{ij}(z^{-1}) = E_i(z^{-1})B_i(z^{-1}) = g_{i0} + g_{i1}z^{-1} \\ + \cdots + g_{i\cdot j-1}z^{-j+1}\ldots \end{aligned} \tag{20}$$

And substitute $G_{ij}(z^{-1})$ and equation (18) into equation (19)

$$\begin{aligned} y_i(k) = F_i(z^{-1})y_i(k-1) + G_{ij}(z^{-1})\Delta u_i(k-1) \\ + E_i(z^{-1})C_i(z^{-1})\xi_i(k) \end{aligned} \tag{21}$$

Assumption 1: The predicted future output value can ignore the influence of noise $\xi_i(k+j)$, then the predicted output variable can be expressed as

$$\hat{y}_i(k+j) = F_i(z^{-1})y_i(k) + G_{ij}(z^{-1})\Delta u_i(k+j-1) \tag{22}$$

Notice that the right side of equation (22) contains two types of variables, the known variable and the unknown variable, at time k, and if using $f_i(k+j)$ to represent the known variable, that is

$$\begin{aligned} \begin{bmatrix} f_i(k+1) \\ f_i(k+2) \\ \vdots \\ f_i(k+j) \end{bmatrix} = \begin{bmatrix} F_{i1} \\ F_{i2} \\ \vdots \\ F_{ij} \end{bmatrix} y_i(k) \\ + \begin{bmatrix} G_{i1} - g_{i0} \\ z(G_{i2} - z^{-1}g_{i1} - g_{i0}) \\ \vdots \\ z^{j-1}(G_{ij} - z^{-j+1}g_{i\cdot j-1} \cdots z^{-1}g_{i1} - g_{i0}) \end{bmatrix} \Delta u_i(k) \end{aligned} \tag{23}$$

Written in matrix form

$$f_i = H_i \Delta u_i(k) + F_i y_i(k) \tag{24}$$

where $H_i = \begin{bmatrix} G_{i1} - g_{i0} \\ z(G_{i2} - z^{-1}g_{i1} - g_{i0}) \\ \vdots \\ z^{j-1}(G_{ij} - z^{-j+1}g_{i\cdot n-1} \ldots z^{-1}g_{i1} - g_{i0}) \end{bmatrix}$
$= \begin{bmatrix} g_{i1}z^{-1} + g_{i2}z^{-2}\ldots \\ g_{i2}z^{-1} + g_{i3}z^{-2}\ldots \\ \vdots \\ g_{ij}z^{-1} + g_{i(j+1)}z^{-2}\ldots \end{bmatrix}$, $F_i = [F_{i1} \quad F_{i2} \quad \cdots \quad F_{ij}]^T$

Then, the compact form of equation (22) can be written as follows

$$\hat{Y}_i = G_{ij}\Delta U_i + f_i \tag{25}$$

where $\hat{Y}_i = [\hat{y}_i(k+1) \quad \hat{y}_i(k+2) \cdots \hat{y}_i(k+j)]^T$,

$$G_{ij} = \begin{bmatrix} g_{i0} & 0 & \cdots & 0 \\ g_{i1} & g_{i0} & \ddots & \vdots \\ \vdots & g_{i\cdot j-1} & \vdots & g_{i\cdot j-2} \\ \ddots & \cdots & 0 & g_{i0} \end{bmatrix},$$

$\Delta U_i = [\Delta u_i(k) \quad \Delta u_i(k+1) \quad \cdots \quad \Delta u_i(k+j-1)]^T$, $f_i = [f_i(k+1) \quad f_i(k+2) \quad \cdots \quad f_i(k+j)]^T$. Besides, G_{ij} denotes square matrix with dimension j of i system.

To make the system outputs reach the set value smoothly, the reference trajectory of the system output is softened, that is

$$w_i(k+j) = \alpha_i^j y_i(k) + \left(1-\alpha_i^j\right) yr_i(k) \tag{26}$$

where $w_i(k)$, $y_i(k)$ and $yr_i(k)$ are reference trajectory, measurement output and input reference, respectively. α_i^j is flexibility coefficient, and $0<\alpha_i^j<1$.

Remark 2: When the reference signal tracked by the system changes greatly, it will bring disturbance to the system. If the reference signal is softened, the disturbance caused by tracking the reference signal with large variation can be avoided. Therefore, $0<\alpha_i^j<1$ represents the degree of softness. The greater the α_i^j, the greater the smoothness. When $\alpha_i^j=0$, we obtain $w_i(k+j) = yr_i(k)((-b \pm \sqrt{b^2-4ac})/2a)$, and the reference signal is not softened. When $0<\alpha_i^j<1$ is selected, α_i^j will gradually approach 0 with the increase in prediction step size j. Therefore, the system can achieve smooth transition by selecting the appropriate α_i^j.

According to equation (26), the reference trajectory of the total j steps from $k+1$ to $k+j$ can be obtained as follows

$$\begin{bmatrix} w_i(k+1) \\ w_i(k+2) \\ \vdots \\ w_i(k+j) \end{bmatrix} = \begin{bmatrix} \alpha_i^1 \\ \alpha_i^2 \\ \vdots \\ \alpha_i^j \end{bmatrix} \cdot y_i(k) + \begin{bmatrix} 1-\alpha_i^1 \\ 1-\alpha_i^2 \\ \vdots \\ 1-\alpha_i^j \end{bmatrix} \cdot yr_i(k) \tag{27}$$

Then, the compact form of equation (27) can be written as follows

$$W_i = Q_i \cdot y_i(k) + M_i \cdot yr_i(k) \tag{28}$$

where $W_i = [w_i(k+1) \quad w_i(k+2) \cdots w_i(k+j)]^T$, $Q_i = [\alpha_i^1 \ \alpha_i^2 \cdots \alpha_i^j]^T$ and $M_i = [1-\alpha_i^1 \ 1-\alpha_i^2 \cdots 1-\alpha_i^j]^T$.

From equation (25), it can be seen that the jth and $(j+1)$ th step predicted output as follows

$$\hat{y}_i(k+j) = G_{ij\cdot j}\Delta u_i(k+j-1) + f_i(k+j) \tag{29}$$

$$\hat{y}_i(k+j+1) = G_{ij+1\cdot j+1}\Delta u_i(k+j) + f_i(k+j+1) \tag{30}$$

where $G_{ij\cdot j}$ and $G_{ij+1\cdot j+1}$ are rows j and $j+1$ of the G_{ij} matrix and G_{ij+1} matrix of i system, respectively.

Then the predicted error at jth step is

$$\hat{e}_i(k+j) = w_i(k+j) - \hat{y}_i(k+j) = \alpha_i^j y_i(k) + y_{ir}(k) - \alpha_i^j y_{ir}(k) - G_{ij\cdot j}\left(z^{-1}\right) \cdot \Delta u_i(k+j-1) - f_i(k+j) \tag{31}$$

The prediction error of step $k+j+1$ is as follows

$$\begin{aligned} \hat{e}_i(k+j+1) &= w_i(k+j+1) - \hat{y}_i(k+j+1) \\ &= yr_i(k) + \alpha_i^{j+1}(y_i(k) - yr_i(k)) - G_{ij+1\cdot j+1} \\ &\quad \Delta u_i(k+j) - f_i(k+j+1) \end{aligned} \tag{32}$$

Referring to the control structure diagram of Figure 1, the error of each system is the sum of the prediction error and the error of the output value of the two systems, that is

$$E_i(k+j) = \hat{e}_i(k+j) + y_s(k+j) - y_I(k+j) \tag{33}$$

$$E_i(k+j+1) = \hat{e}_i(k+j+1) + y_s(k+j+1) - y_I(k+j+1) \tag{34}$$

Sliding mode predictive controller

We can obtain from equation (33) that the predicted sliding mode surface is

$$\hat{s}_i(k+j) = c_{i1} \cdot E_i(k+j) \tag{35}$$

where $c_{i1} > 0$.

Then the predicted sliding mode surface of $\hat{s}_i(k+j+1)$ is

$$\hat{s}_i(k+j+1) = c_{i1} \cdot E_i(k+j+1) \tag{36}$$

To make the system reach the sliding surface quickly, an NMRL composed of exponential reaching law and double power reaching law is designed. The new approach rate NMRL is as follows

$$\begin{aligned} \hat{s}_i(k+j+1) - \hat{s}_i(k+j) &= -T_i k_{i1} \hat{s}_i(k+j) \\ &\quad - (T_i k_{i2} |\hat{s}_i(k+j)|^{\alpha_{i1}} - T_i k_{i3} |\hat{s}_i(k+j)|^{\alpha_{i2}}) sgn(\hat{s}_i(k+j)) \end{aligned} \tag{37}$$

where T_i is the sampling time of i system, $k_{i1}>0, k_{i2}>0, k_{i3}>0, 0<\alpha_{i1}<1, 1<\alpha_{i2}<2$.

Remark 3: When $|\hat{s}_i(k+j)|<1$, the second term plays a dominant role to ensure that the system state quickly reaches the sliding surface. When $|\hat{s}_i(k+j)|>1$, the third term plays a leading role to ensure that the system state quickly reaches the sliding surface. And in general, α_{i1} and α_{i2} satisfy $\alpha_{i1}+\alpha_{i2}=2$.

Subtract equation (35) from equation (36) to get

$$\begin{aligned} \hat{s}_i(k+j+1) - \hat{s}_i(k+j) &= c_{i1}[E_i(k+j+1) - E_i(k+j) \\ &= c_{i1}[y_i(k)(\alpha_i^{j+1} - \alpha_i^j) - yr_i(k)(\alpha_i^{j+1} - \alpha_i^j) \\ &\quad + f_i(k+j) - f_i(k+j+1) + G_{ij\cdot j}\Delta u_i(k+j-1) \\ &\quad - G_{ij+1\cdot j+1}\Delta u_i(k+j) + y_s(k+j+1) \\ &\quad - y_I(k+j+1) - y_s(k+j) + y_I(k+j)] \end{aligned} \tag{38}$$

According to equations (37) and (38), it is not difficult to derive the control law as follows

$$u_i(k+j) = G_{ij+1,j+1}{}^{-1}\Big[y_i(k)\Big(\alpha_i^{j+1} - \alpha_i^j\Big) - \alpha_i^{j+1}yr_i(k) + \alpha_i^j yr_i(k) + f_i(k+j) - f_i(k+j+1) - y_s(k+j) + y_I(k+j) + G_{ij,j}\Delta u_i(k+j-1) + y_s(k+j+1) - y_I(k+j+1) + (c_{i1}G_{ij+1,j+1})^{-1}(T_i k_{i1}\hat{s}_i(k+j) + (T_i k_{i2}|\hat{s}_i(k+j)|^{\alpha_{i1}} + T_i k_{i3}|\hat{s}_i(k+j)|^{\alpha_{i2}})sgn(\hat{s}_i(k+j))\Big] + u_i(k+j-1) \tag{39}$$

Remark 4: Compared with the traditional sliding mode control algorithm, NSMP control scheme has prediction function and can predict the state change of the system in TD. Compared with the existing sliding mode prediction results, the NMPC structure is simpler and does not need to calculate the minimization cost function. It does not need an accurate mathematical model of the system and can improve the generality on the premise of improving the control accuracy.

Theorem 1 (stability): For the photoelectric imaging system (4), considering the predictive sliding mode surface (35) and the predictive controller (39), the states of system (4) converge to the switching surface $s = 0$ and thereafter stay on it, satisfying the following inequality

$$0 < 1 - T_i k_{i1} G_{ij+1,j+1}{}^{-1} < 1 \tag{40}$$

Proof: According to the discrete SMC theory, the discrete SMC makes the state motion of the system monotonically approach the sliding mode surface at first, but it does not cross the sliding mode surface in the process of reaching. When the approach process passes through the sliding surface once, then every step will pass through the other side of the sliding surface and go on. At this time, the system enters the quasi sliding mode.

Substituting equation (39) into equation (30), and combining equations (31), (32), (35), (36) and (37), one gets

$$\hat{s}_i(k+j+1) = \left(1 - T_i k_{i1} G_{ij+1,j+1}{}^{-1}\right)\hat{s}_i(k+j) - G_{ij+1,j+1}{}^{-1}[T_i k_{i2}|\hat{s}_i(k+j)|^{\alpha_{i1}} + T_i k_{i3}|\hat{s}_i(k+j)|^{\alpha_{i2}}]sgn(\hat{s}_i(k+j)) \tag{41}$$

In the process of photoelectric imaging system approaching the predicted sliding mode surface, the positive and negative of $\hat{s}_i(k+j+1)$ and $\hat{s}_i(k+j)$ are the same. For equation (41), it needs to be considered in two cases:

When $\hat{s}_i(k+j) > 0$ and equation (38) is considered, we have

$$\begin{aligned}\hat{s}_i(k+j+1) &= \left(1 - T_i k_{i1} G_{ij+1,j+1}{}^{-1}\right)\hat{s}_i(k+j) \\ &- G_{ij+1,j+1}{}^{-1}[T_i k_{i2}|\hat{s}_i(k+j)|^{\alpha_{i1}} + T_i k_{i3}|\hat{s}_i(k+j)|^{\alpha_{i2}}] \\ &< \left(1 - T_i k_{i1} G_{ij+1,j+1}{}^{-1}\right)\hat{s}_i(k+j) < \hat{s}_i(k+j)\end{aligned} \tag{42}$$

When $\hat{s}_i(k+j) < 0$ and equation (41) is considered, we get

$$\begin{aligned}\hat{s}_i(k+j+1) &= \left(1 - T_i k_{i1} G_{ij+1,j+1}{}^{-1}\right)\hat{s}_i(k+j) \\ &+ G_{ij+1,j+1}{}^{-1}[T_i k_{i2}|\hat{s}_i(k+j)|^{\alpha_{i1}} + T_i k_{i3}|\hat{s}_i(k+j)|^{\alpha_{i2}}] \\ &> \left(1 - T_i k_{i1} G_{ij+1,j+1}{}^{-1}\right)\hat{s}_i(k+j) > \hat{s}_i(k+j)\end{aligned} \tag{43}$$

According to the proof of the above two cases, we can have

$$|\hat{s}_i(k+j+1)| < \left|\left(1 - T_i k_{i1} G_{ij+1,j+1}{}^{-1}\right)\hat{s}_i(k+j)\right| < |\hat{s}_i(k+j)| \tag{44}$$

Therefore, the photoelectric imaging system satisfies the arrival condition of discrete sliding mode, that is, the system state can reach the sliding mode surface, so the motion state of system can converge to zero.

Theorem 2 (Finite time convergence): In the target tracking process of the photoelectric imaging system, the discrete sliding mode predictive controller (39) can make the system converge in finite time, and the convergence rate is inversely proportional to k_{i1}.

Proof: Before reaching the predicted sliding mode surface, from equation (44) one obtains

$$[\hat{s}_i(k+j+1) - \hat{s}_i(k+j)]\hat{s}_i(k+j) < -T_i k_{i1} G_{ij+1,j+1}{}^{-1}\hat{s}_i(k+j)^2 \tag{45}$$

And then

$$|\hat{s}_i(k+j+1)| < |\hat{s}_i(k+j)| - T_i k_{i1} G_{ij+1,j+1}{}^{-1}|\hat{s}_i(k+j)| \tag{46}$$

$\hat{s}_i(0)$ is defined as the initial value of sliding surface; therefore

$$\hat{s}_i(k+j) < \hat{s}_i(0) \tag{47}$$

Simultaneously considering equations (46) and (47), one has

$$\begin{aligned}|\hat{s}_i(k+j+1)| &< |\hat{s}_i(k+j)| - T_i k_{i1} G_{ij+1,j+1}{}^{-1}|\hat{s}_i(k+j)| \\ &< |\hat{s}_i(0)| - k \cdot T_i k_{i1} G_{ij+1,j+1}{}^{-1}|\hat{s}_i(0)|\end{aligned} \tag{48}$$

When the sign of $\hat{s}_i(k+j+1)$ is the same as that of $\hat{s}_i(k+j)$, equation (51) is tenable. However, there must be a natural number N so that when $k \geq N$, the right side of equation (48) is $|\hat{s}_i(0)| - N \cdot T_i k_{i1} G_{ij+1,j+1}{}^{-1}|\hat{s}_i(0)| < 0$, implying $|\hat{s}_i(k+j+1)| < 0$, which is impossible. This shows that the value of $\hat{s}_i(N+j+1)$ must be different from the value of $\hat{s}_i(0)$, so it means that the prediction error will enter the sliding surface in finite steps, that is to say, the prediction error can converge in finite time.

According to the above analysis, when $|\hat{s}_i(N+j+1)| < 0, |\hat{s}_i(N+j)| > 0$; therefore

$$|\hat{s}_i(0)| - N \cdot T_i k_{i1} G_{ij+1,j+1}{}^{-1}|\hat{s}_i(0)| > 0 \tag{49}$$

$$T^* < \frac{G_{ij+1,j+1}}{k_{i1}} \tag{50}$$

To sum up, the prediction error will converge in finite time T^*. It can be seen from equation (50) that the larger the k_{i1}, the faster the convergence speed, and the proof is completed.

Assumption 2: The maximum value of initial value $|\hat{s}_i(0)|$ of sliding surface is less than $\beth$.

Assumption 3: The maximum value of $|\hat{s}_i(k+j)|$ is greater than positive integer 1.

Theorem 3 (error boundedness): Consider systems (1)–(4) and satisfy Assumption 1. For NSMP, there exists a constant $\ell > 0$, such that for

$$|E_i(k+j+1)| < l \tag{51}$$

where $\ell = \sqrt{(1+\varrho))\beth^2 + \delta\beth^4}/\mathrm{c}_{i1}$.

Proof: Consider equations (40) and (41), such that for

$$\begin{aligned}
&[\hat{s}_i(k+j+1) + \hat{s}_i(k+j)][\hat{s}_i(k+j+1) - \hat{s}_i(k+j)] \\
&= -T_i k_{i1}(2 - T_i k_{i1})|\hat{s}_i(k+j)|^2 + (T_i k_{i2})^2 |\hat{s}_i(k+j)|^{2\alpha_{i1}} \\
&- 2T_i k_{i2}(1 - T_i k_{i1})|\hat{s}_i(k+j)|^{1+\alpha_{i1}} \\
&- 2T_i k_{i3}(1 - T_i k_{i1})|\hat{s}_i(k+j)|^{1+\alpha_{i2}} + 2T_i^2 k_{i2} k_{i3} |\hat{s}_i(k+j)|^{\alpha_{i1}+\alpha_{i2}} \\
&+ (T_i k_3)^2 |\hat{s}_i(k+j)|^{2\alpha_{i2}}
\end{aligned} \tag{52}$$

According to Assumption 2, $|\hat{s}_i(k+j)| > 1$. If we enlarge it properly, we get

$$\begin{aligned}
&|\hat{s}_i(k+j+1)|^2 - |\hat{s}_i(k+j)|^2 < 2T_i^2 k_{i2} k_{i3} |\hat{s}_i(k+j)|^2 \\
&+ (T_i k_{i2})^2 |\hat{s}_i(k+j)|^2 - 2T_i k_{i3}(1 - T_i k_{i1})|\hat{s}_i(k+j)|^2 \\
&- 2T_i k_{i1}(1 - T_i k_{i1})|\hat{s}_i(k+j)|^2 + (T_i k_3)^2 |\hat{s}_i(k+j)|^4 \\
&= [2T_i^2 k_{i2} k_{i3} + (T_i k_{i2})^2 - 2T_i k_{i3}(1 - T_i k_{i1}) - 2T_i k_{i1}(1 - T_i k_{i1})] \\
&\quad |\hat{s}_i(k+j)|^2 + (T_i k_3)^2 |\hat{s}_i(k+j)|^4
\end{aligned} \tag{53}$$

Then, one gets

$$\begin{aligned}
&|\hat{s}_i(k+j+1)|^2 < \Big(1 + 2T_i^2 k_{i2} k_{i3} + (T_i k_{i2})^2 - 2T_i k_{i3}(1 - T_i k_{i1}) - 2T_i k_{i1}(1 - T_i k_{i1})\Big)()|\hat{s}_i(k+j)|^2 \\
&+ (T_i k_3)^2 |\hat{s}_i(k+j)|^4 < \Big(1 + 2T_i^2 k_{i2} k_{i3} + (T_i k_{i2})^2 - 2T_i k_{i3}(1 - T_i k_{i1}) - 2T_i k_{i1}(1 - T_i k_{i1})\Big)\beth^2 + (T_i k_3)^2 \beth^4
\end{aligned} \tag{54}$$

Let $[2T_i^2 k_{i2} k_{i3} + (T_i k_{i2})^2 - 2T_i k_{i3}(1 - T_i k_{i1}) - 2T_i k_{i1}(1 - T_i k_{i1})] = \varrho$ and $(T_i k_3)^2 = \delta$. Then we have $|\hat{s}_i(k+j+1)| < \sqrt{(1+\varrho))\beth^2 + \delta\beth^4}$. Then, considering equation (36), one obtains

$$|E_i(k+j+1)| < \sqrt{(1+\varrho))\beth^2 + \delta\beth^4}/c_{i1} \tag{55}$$

Let $\frac{\sqrt{(1+\varrho))\beth^2 + \delta\beth^4}}{\mathrm{c}_{i1}} = \ell$. Then, the conclusion in equation (51) holds.

Corollary 1: According to Theorem 1 and Theorem 3, when $k \to \infty$, $E_i(k+j+1) \to 0$ with an exponential rate.

Remark 5: Theorem 1 shows the proposed NSMP can make the error converge stably. Theorem 2 further shows the upper limit of convergence time of the error. Theorem 3 and Corollary 1 quantify the error upper bound and show that the error converges exponentially.

Power function analysis

In fact, the switch function $sgn(\hat{s}_i(k+j))$ would cause excessive switching of control law $u_i(k+j)$. Consequently, it leads to the chattering problem of the system. Therefore, the method of continuous approach is usually used to weaken the chattering of the system, and the power function $fal[\hat{s}_i(k+j)]$ is developed to replace the switch function $sgn(\hat{s}_i(k+j))$ and then $fal[\hat{s}_i(k+j)]$ as follows

$$fal[(\hat{s}_i(k+j)] = \begin{cases} arctan[\hat{s}_i(k+j)], |\hat{s}_i(k+j)| \le \rho \\ \rho^{-1} \cdot \hat{s}_i(k+j), |\hat{s}_i(k+j)| > \rho \end{cases} \tag{56}$$

where ρ represents the boundary layer, and $0 < \rho < 1$. $0 < \rho < 1$, the power function of the control law is $arctan[\hat{s}_i(k+j)]$ function inside the boundary layer, which can weaken the chattering of the system. The power function is $\rho^{-1} \cdot \hat{s}_i(k+j)$ outside the boundary layer. Due to $0 < \rho < 1$, it can increase the convergence speed and tracking accuracy of the system by selecting the appropriate ρ.

Remark 6: $fal[(\hat{s}_i(k+j)]$ and $sgn(\hat{s}_i(k+j))$ are the same positive and negative, so the replacement does not affect the stability of the system.

Experimental simulation and analysis

The proposed algorithm is implemented and evaluated on a discrete photoelectric imaging system. The objective is to perform stable imaging control while tracking trajectory in the presence of TD and disturbances.

Comparative analysis of disturbance compensation strategies

To verify the effectiveness of the disturbance compensation control strategy proposed in this paper, the traditional DOB is used, compared with the RDOB. The experimental analysis is carried out using a low-frequency disturbance $d(k) = 0.1sin(5\pi kT)$ and a high-frequency disturbance

$d(k) = 0.1 sin(15\pi kT)$, respectively, to the system. To more clearly observe the simulation image of the above contrast scheme, taking the scanning mirror motor as an example and the sampling period as $T = 0.002$ s, the discrete model of the motor is as follows

$$A_s(z^{-1})y_s(k) = B_s(z^{-1})u_s(k-1) + C_s(z^{-1})\xi_s(k)/\Delta \tag{57}$$

where $A_s(z^{-1}) = 1 - 1.607z^{-1} + 0.6065z^{-2}$, $B_s(z^{-1}) = 0.2983 + 0.2526z^{-1}$ and $C_s(z^{-1}) = 1$.

According to the selection rule of weight function in RHMS control theory, the weight function is selected as

$$W_{ss}(z^{-1}) = \frac{0.6667 - 0.3667z^{-1}}{1 - z^{-1}} \tag{58}$$

$$W_{sks}(z^{-1}) = 1 \tag{59}$$

Then the suboptimal solution is calculated as $\gamma = 0.98$ through the MATLAB robust toolbox, and finally the robust controller is obtained as follows

$$K_s(z^{-1}) = \frac{1.443 \times z^{-1} - 1.365 \times 10^{-4} z^{-2} + 3.405 \times 10^{-20} \times z^{-3}}{1 - 7.5 \times 10^{-5} \times z^{-1} - 3.957 \times 10^{-19} \times z^{-2} - 1.742 \times 10^{-32} \times z^{-3}} \tag{60}$$

The filter of traditional disturbance observer is: $Q_S(z^{-1}) = (0.04207 + 0.09466z^{-1} + 0.0631z^{-2} + 0.01052z^{-3})/(1 - 0.886z^{-1} - 0.8494z^{-2} + 0.9457z^{-3})$

As shown in Figure 4(a) and (b), both interference estimation strategies have good estimation accuracy and speed. In the case of low-frequency disturbance, the estimation accuracy of the proposed compensation strategy in this paper and the traditional DOB is $\delta = 4 \times 10^{-4}$ and $\delta = 2 \times 10^{-3}$, respectively. In the case of high-frequency disturbance, the estimation accuracy of the proposed compensation strategy in this paper and the traditional DOB is $\delta = 1.3 \times 10^{-3}$ and $\delta = 7 \times 10^{-3}$, respectively. Therefore, it can be seen that the RDOB has higher estimation accuracy, which demonstrates that the disturbance compensation control strategy proposed in this paper is effective.

In addition, Zhou et al. (1995) proved that the smaller the value of γ, the higher the control accuracy of the system under the condition of ensuring the stability of the system. To understand the influence of γ value on the system control accuracy more clearly and intuitively, we conducted the simulation experiments when $\gamma = 0.98$ and $\gamma = 1.065$, respectively. It can be seen from Figure 5 that the disturbance estimation accuracy of $\gamma = 0.98$ is higher than that of $\gamma = 1.065$. Therefore, the smaller the value of γ, the higher the estimation accuracy of the system in the case of ensuring the stability of the system.

Comparative analysis of predictive control schemes for systems with TD

To verify the effectiveness of NSMP, three groups of simulation experiments are carried out in this section. The first group is the simulation experiment of the slide mode control strategy based on NMRL without introducing generalized prediction control, the second group is the simulation experiment of the control strategy proposed in Liu et al. (2020) and the third group is the simulation experiment of the control strategy proposed in this paper.

As analysed earlier, there is about 20 ms delay in the position feedback channel of the imaging system. To simulate the real control environment, a delay of 20 ms is added at the same time of given and scanning mirror position detection, as shown in T2 in Figure 1. Because the sampling period is 0.002 s, the delay of 20 ms can be regarded as 10 steps lag. Therefore, it is necessary to predict the same number of steps to reduce the error. And then there are the predicted steps $j = 10$. In addition, to better verify the effectiveness of the control strategy, random white noise with standard deviation of 0.01 is added to the measurement output.

NMRL control rate without prediction function is as follows

$$\begin{aligned} u_c(k-1) = {} & b_{s0}^{-1}[-Tk_{c1}c_c^{-1}s(k) - w_{sc}(k-1) \\ & - Tk_{c2}c_c^{-1}|s(k)|^{\alpha_{c1}} fal(s(k)) + w_{sc}(k) - Tk_{c3}c_c^{-1}|s(k)|_{c2}^{\alpha}|fal] \\ & (s(k)) - a_{s2}y(k-1) - b_{s1}u_c(k-2) \end{aligned} \tag{61}$$

where $\alpha_c = 0.09, c_c = 0.09$, $k_{c1} = 0.9$, $k_{c2} = 2$, $k_{c3} = 0.01$, $\alpha_{c1} = 0.3$, $\alpha_{c2} = 1.7$ and $\rho = 0.1$. The controller parameters of NSMP are $\alpha_s = 0.01$, $c_s = 1$, $k_{s1} = 1$, $k_{s2} = 10$, $k_{s3} = 10$, $\alpha_{s1} = 0.4$, $\alpha_{s2} = 1.6$ and $\rho_s = 0.2$, and the simulation results are as follows.

It can be seen from (a) in Figures 6–8 that predictive control can effectively weaken the impact of TD. It can be seen from (b) in Figures 6–8 that the tracking accuracy of the three groups of experiments is $\delta = 0.35$, 3×10^{-4} and 5×10^{-5} respectively. It can be seen from (c) in Figures 6–8 that the control accuracy of the three groups of experiments is $\delta = 0.3$, $\delta = 0.03$ and $\delta = 1 \times 10^{-3}$ respectively. Compared with the first group of simulation experiments, the second and third group of simulation experiments can find that the introduction of prediction algorithm can effectively overcome the TD. Compared with the second group of simulation experiments, the third group of simulation experiments can find that the proposed control algorithm has higher tracking accuracy in the presence of TD and external disturbance.

Comparative study of image rotation–suppressed control schemes

The following experimental work will show that control method proposed in this paper can effectively solve the image rotation problem in the airborne photoelectric tracking system.

The scanning system model is shown in equation (57), and the discrete model of the imaging detector system is as follows

$$A_I(z^{-1})y_I(k) = B_I(z^{-1})u_I(k-1) + C_I(z^{-1})\xi_I(k)/\Delta \tag{62}$$

where $A_I(z^{-1}) = 1 - 1.558z^{-1} + 0.558z^{-2}$, $B_I(z^{-1}) = 0.2908 + 0.2395z^{-1}$ and $C_I(z^{-1}) = 1$.

The controller parameter settings are $\alpha_I = 0.0001$, $c_I = 1.7$, $k_{I1} = 26.4$, $k_{I2} = 10$, $k_{I3} = 15$, $\alpha_{I1} = 0.8$, $\alpha_{I2} = 1.2$

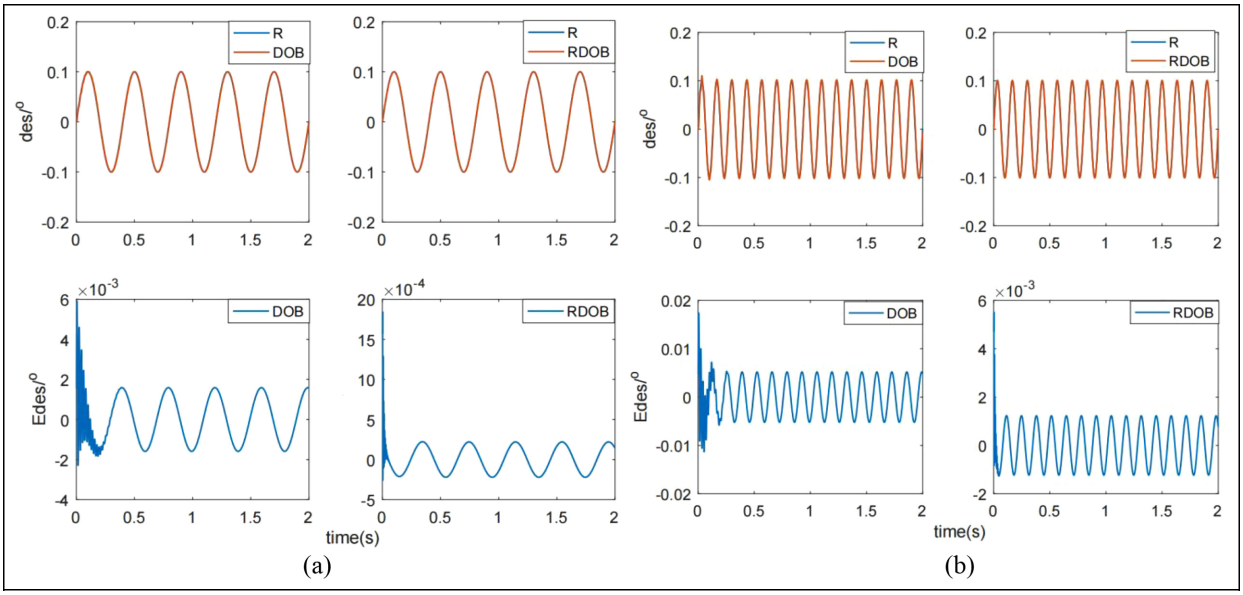

Figure 4. Disturbance estimation and estimation error curve: (a) low frequency and (b) high frequency.

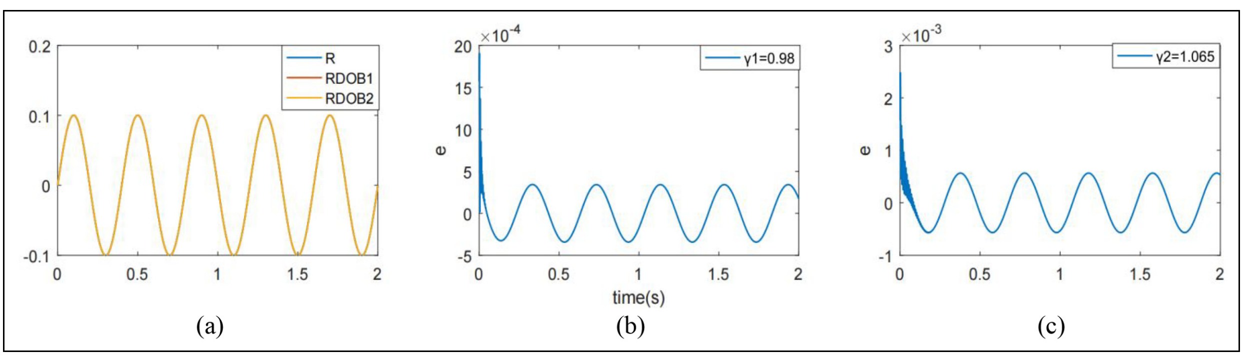

Figure 5. (a) Different γ value estimation curve. (b) $\gamma = 0.98$ disturbance estimation curve. (c) $\gamma = 1.065$ disturbance estimation curve.

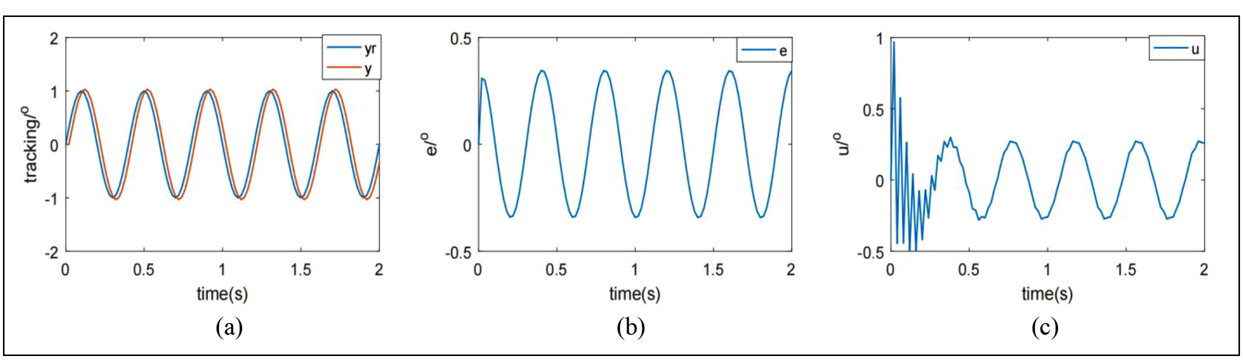

Figure 6. NMRL control strategy simulation curve: (a) tracking curve; (b) tracking error curve; (c) control output curve.

and $\rho_I = 0.25$. For comparative simulation, in traditional tracking mode the controller parameter settings for the scanning mirror system and the imaging system are $\alpha_s = 0.5$, $c_s = 900$, $k_{s1} = 900$, $k_{s2} = 150$, $k_{s3} = 700$, $\alpha_{s1} = 0.9$, $\alpha_{s2} = 1.1$, $\rho_s = 0.5$, $\alpha_I = 0.01$, $c_I = 2$, $k_{I1} = 700$, $k_{I2} = 100$, $k_{I3} = 15$, $\alpha_{I1} = 0.8$, $\alpha_{I2} = 1.2$ and $\rho_I = 0.3$. The comparative

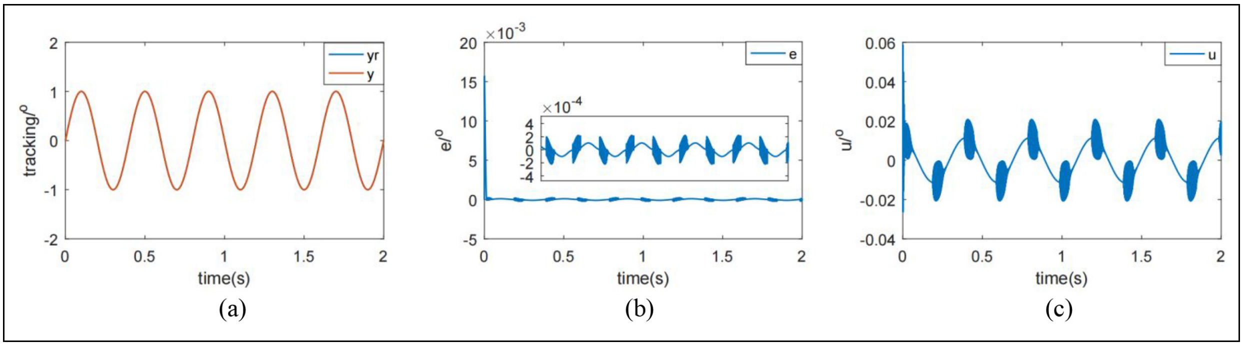

Figure 7. Liu et al.'s (2020) control strategy simulation curve: (a) tracking curve; (b) tracking error curve; (c) control output curve.

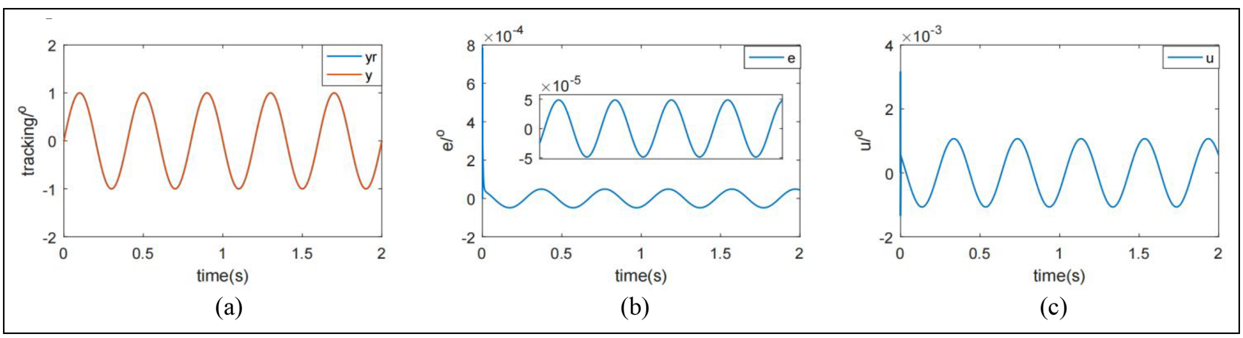

Figure 8. NSMP control strategy simulation curve: (a) tracking curve; (b) tracking error curve; (c) control output curve.

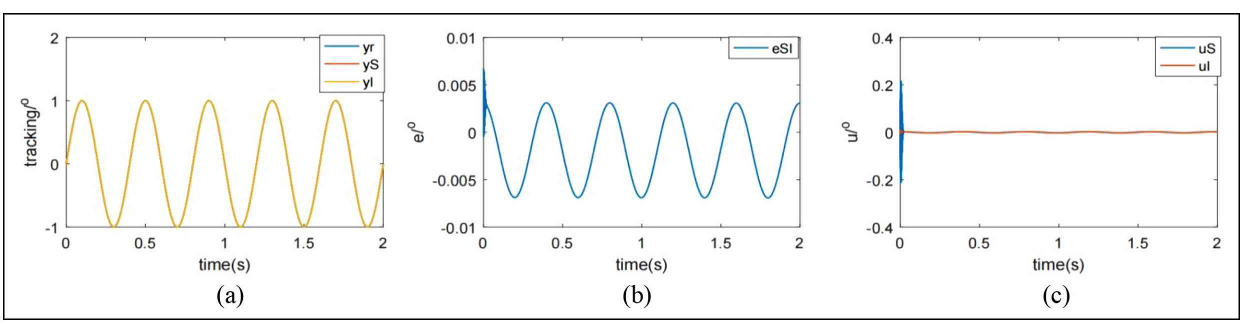

Figure 9. Traditional control structure: (a)tracking curve; (b) tracking error curve; (c) control output curve.

simulation results of bilateral control structure and traditional unilateral structure are shown in Figures 9 and 10.

It can be seen from (b) in Figures 9 and 10 that the synchronization accuracy of the traditional control structure and bilateral control structure is $\delta = 7 \times 10^{-3}$ and 5×10^{-4}, respectively. It can be seen from (c) in Figures 9 and 10 that the control accuracy of the traditional control structure and bilateral control structure is $\delta = 5 \times 10^{-3}$ and $\delta = 1.5 \times 10^{-3}$, respectively. Therefore, we can see that the image rotation compensation accuracy of the NSMP based on the bilateral control structure is higher than that of the traditional control method, which effectively alleviates the non-synchronous problem between the scanning mirror and the imaging detector that causes image rotation.

Conclusion

To achieve high-precision stable imaging in the photoelectric imaging system, a bilateral control structure is used to overcome the image rotation problem. In this control structure, the control method combining disturbance compensation

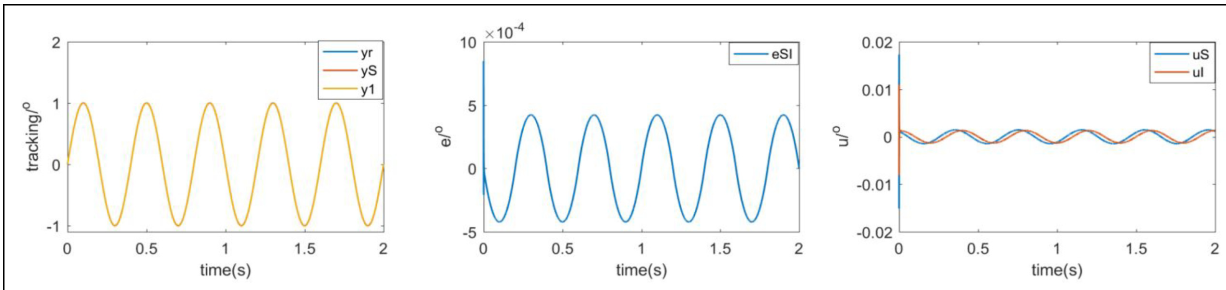

Figure 10. Bilateral control structure: (a) tracking curve; (b) tracking error curve; (c) control output curve.

control strategy with tracking control strategy is proposed and applied to ensure the robustness of the system and improve the tracking accuracy of the system. For the disturbance compensation control strategy, RDOB is developed to eliminate the equivalent disturbances. For the tracking control strategy, NSMP is proposed to solve the TD problem of the system and achieve high-precision tracking control, in which a new power function is designed to replace the switching function to weaken the chattering problem in sliding mode control. In the aspect of theoretical analysis, by using Lyapunov theory and finite time theory, it is proved that the controller designed in this paper can make the system stable in finite time. And finally, simulation experiment is carried out to verify the effectiveness of the control method. The control scheme in this paper is also applicable to other photoelectric tracking systems

With the rapid development of communication technology, the cooperative control among multiple photoelectric imaging systems will be the general research direction of development in the future. Its information measurement and estimation can be transmitted through the communication network to improve the flexibility of the system. However, communication networks have their own limitations, such as bandwidth limitation and vulnerability to network attacks. Therefore, it is one of the future works to study how to design a reliable and safe estimation/control method for the cooperative control of multiple photoelectric imaging system with network attack.

Declaration of conflicting interests

The author(s) declared no potential conflicts of interest with respect to the research, authorship and/or publication of this article.

Funding

The author(s) disclosed receipt of the following financial support for the research, authorship and/or publication of this article: This work was supported by the National Natural Science Foundation of China (No. 62063027, No. 61673365), Science and technology planning project of Inner Mongolia Autonomous Region (2020GG0048), Support Program for Young Talents of Science and Technology in Universities of Inner Mongolia Autonomous Region (NJYT22057), Key Laboratory of Airborne Optical Imaging and Measurement of Chinese Academy of Sciences Open Foundation (HCKF-201912).

ORCID iD

Wang Yimin https://orcid.org/0000-0002-7476-6805

References

Bentsman J and Ordys A (1999) Ill-posedness and Ill-conditioning in the use of CARMA, CARIMA and Box-Jenkins models in identification and control. In: *1999 European control conference*, Karlsruhe, 31 August–3 September.

Cecilia A, Sahoo S, Dragicevic T, et al. (2021) Detection and mitigation of false data in cooperative dc microgrids with unknown constant power loads. *IEEE Transactions on Power Electronics* 36(8): 9565–9577.

Chang T, Wang Q, Zhang L, et al. (2019) Battlefield dynamic scanning and staring imaging system based on fast steering mirror. *Journal of Systems Engineering and Electronics* 30(1): 37–56.

Chen X, Li Y, Ma H, et al. (2021) A novel variable exponential discrete time sliding mode reaching law. *IEEE Transactions on Circuits and Systems II: Express Briefs* (68)7: 2518–2522.

Chen Z, Huang F, Yang C, et al. (2020) Adaptive fuzzy back-stepping control for stable nonlinear bilateral teleoperation manipulators with enhanced transparency performance. *IEEE Transactions on Industrial Electronics* 67(1): 746–756.

Ding S, Chen WH, Mei K, et al. (2020) Disturbance observer design for nonlinear systems represented by input-output models. *IEEE Transactions on Industrial Electronics* 67(2): 1222–1232.

Fan C, Xie Z, Liu Y, et al. (2020) Manipulator trajectory tracking of fuzzy control based on spatial extended state observer. *IEEE Access* 8: 24296–24308.

Fang M, Shi P and Dong S (2021) Sliding mode control for Markov jump systems with delays via asynchronous approach. *IEEE Transactions on Systems, Man, and Cybernetics: Systems* 51(5): 2916–2925.

Gao J, Gong C, Li W, et al. (2020) Novel compensation strategy for calculation delay of finite control set model predictive current control in PMSM. *IEEE Transactions on Industrial Electronics* 67(7): 5816–5819.

Giuffrida MV and Tsaftaris SA (2020) Unsupervised rotation factorization in restricted Boltzmann machines. *IEEE Transactions on Image Processing* 29(1): 2166–2175.

Han X (2021) Linear matrix inequalities-based adaptive time-delayed sliding mode control for ships considering ship-bank interaction effect and shallow water effect. *Asian Journal of Control* 24(4): 1780–1794.

Huerta H and Loukianov A (2021) Energy based sliding mode control of brushless double-fed induction generator. *International Journal of Electrical Power & Energy Systems* 130(403): 107002.

Hu R, Deng H and Zhang Y (2020) Novel dynamic-sliding-mode-manifold-based continuous fractional-order nonsingular terminal sliding mode control for a class of second-order nonlinear systems. *IEEE Access* 8: 19820–19829.

Labbadi M and Moussaoui HE (2021) An improved adaptive fractional-order fast integral terminal sliding mode control for distributed quadrotor. *Mathematics and Computers in Simulation* 188: 120–134.

Liu YC, Dao PN and Zhao KY (2020) On robust control of nonlinear tele-operators under dynamic uncertainties with variable time delays and without relative velocity. *IEEE Transactions on Industrial Informatics* 16(2): 1272–1280.

Mobayen S (2018) Synchronization of a class of uncertain chaotic systems with Lipschitz nonlinearities using state-feedback control design: A matrix inequality approach. *Asian Journal of Control* 20(1): 71–85.

Mobayen S and Tchier F (2017) Composite nonlinear feedback control technique for master/slave synchronization of nonlinear systems. *Nonlinear Dynamics* 87(3): 1–17.

Ogunye AB (1999) Solution of unilateral and bilateral Diophantine equations using symbolic computation. In: *IEEE international symposium on computer aided control system design*, Kohala Coast, HI, 27 August.

Ovaska SJ and Vainio O (1997) Predictive compensation of time-varying computing delay on real-time control systems. *IEEE Transactions on Control Systems Technology* (5)5: 523–526.

Ren Y, Tian D and Yu D (2020) Research of NSMDOB-based compound control for photoelectric tracking platform. *IEEE Access* 8: 62650–62659.

Tajiri M, Lopez P and Fujimoto Y (2018) Design of two-channel bilateral control systems by a transfer-function-based approach. *IEEE Transactions on Industrial Electronics* 65(7): 5655–5664.

Teng L, Wang Y, Cai W, et al. (2019) Efficient robust fuzzy model predictive control of discrete nonlinear time-delay systems via Razumikhin approach. *IEEE Transactions on Fuzzy Systems* 27(2): 262–272.

Tian D, Wang Y, Wang F, et al. (2015) Bilateral control-based compensation for rotation in imaging in scan imaging systems. *Optical Engineering* 54(12): 183–183.

Truong DQ, Ahn KK and Trung NT (2013) Design of an advanced time delay measurement and a smart adaptive unequal interval grey predictor for real-time nonlinear control systems. *IEEE Transactions on Industrial Electronics* 60(10): 4574–4589.

Ullah I and Pei HL (2020) Fixed time disturbance observer based sliding mode control for a miniature unmanned helicopter hover operations in presence of external disturbances. *IEEE Access* 8: 73173–73181.

Wang P, Zhu C and Gao J (2019a) Feedforward model predictive control of fuel-air ratio for lean-burn spark-ignition gasoline engines of passenger cars. *IEEE Access* 7: 73961–73969.

Wang Y, Feng Y, Zhang X, et al. (2019b) New reaching law control for permanent magnet synchronous motor with extended disturbance observer. *IEEE Access* 7: 186296–186307.

Wang Y, Feng Y, Zhang X, et al. (2020) A new reaching law for anti-disturbance sliding-mode control of PMSM speed regulation system. *IEEE Transactions on Power Electronics* 35(4): 4117–4126.

Xia Y and Jia Y (2003) Robust sliding-mode control for uncertain time-delay systems: An LMI approach. *IEEE Transactions on Automatic Control* 48(6): 1086–1091.

Yang P, Liu Z, Li D, et al. (2020) Sliding mode prediction fault-tolerant control method for multi-delay uncertain discrete system with sensor fault. *Transactions of the Institute of Measurement and Control* 43(2): 262–272.

Yao J, Saito M, Okada S, et al. (2014) Erela: A low-power reliable coarse-grained reconfigurable architecture processor and its irradiation tests. *IEEE Transactions on Nuclear Science* 61(6): 3250–3257.

Yao W, Wang Y, Xu Y, et al. (2022) Distributed weight-average-prediction control and stability analysis for an islanded microgrid with communication time delay. *IEEE Transactions on Power Systems* 37(1): 330–342.

Zhang J, Chai SC, Zhang BH, et al. (2021a) Distributed model-free sliding-mode predictive control of discrete-time second-order nonlinear multi-agent systems with delays. *IEEE Transactions on Cybernetics* 57(10): 2231–2241.

Zhang J, Liu Y, Zhang F, et al. (2019a) Digital sliding mode control via a novel reaching law and application in shipborne electro-optical systems. *IEEE Access* 7: 139870–139884.

Zhang Y, Xie S, Ren LT, et al. (2019b) A new predictive sliding mode control approach for networked control systems with time delay and packet dropout. *IEEE Access* 7: 134280–134292.

Zhang Z, Yang P, Hu X, et al. (2021b) Sliding mode prediction fault-tolerant control of a quad-rotor system with multidelays based on ICOA. *International Journal of Innovative Computing, Information and Control* 17(1): 49–66.

Zhou K, Doyle JC and Glover K (1995) *Robust and Optimal Control*. London: Springer.